Engineering Stability of the Insulin Monomer Fold with Application to Structure–Activity Relationships

Niels C. Kaarsholm,* Kjeld Norris, Rikke J. Jørgensen, Jørgen Mikkelsen, Svend Ludvigsen, Ole H. Olsen, Anders R. Sørensen, and Svend Havelund

Novo Research Institute, Novo Nordisk A/S, DK-2880 Bagsvaerd, Denmark

Received May 18, 1993; Revised Manuscript Received July 13, 1993®

ABSTRACT: To evaluate the possible relationship between biological activity and structural stability in selected regions of the insulin molecule, we have analyzed the guanidine hydrochloride induced reversible unfolding of a series of mutant insulins using a combination of near- and far-UV circular dichroism (CD). The unfolding curves are reasonably described on the basis of a two-state denaturation scheme; however, the observation of subtle differences between near- and far-UV CD detected unfolding indicates that intermediates may be present. Three regions of the insulin molecule are analyzed in detail with respect to their contribution to folding stability, i.e., the central B-chain helix, the NH_2-terminal A-chain helix, and the B25–B30 extended chain region. Considerable enhancement of folding stability is engineered by mutations at the N-cap of the central B-chain helix and at the C-cap of the NH_2-terminal A-chain helix. Mutations that confer increased stability in these regions are identical to those that lead to enhanced biological activity. In contrast, for insulin species modified in the B25–B30 region of the molecule, we observe no correlation between global folding stability and bioactivity. Mutations in the three regions examined are found to affect stability in a nearly independent fashion, and stabilizing mutations are generally found to enhance the cooperativity of the unfolding transition. We conclude that highly potent insulins (i.e., HisA8, ArgA8, GluB10, and AspB10) elicit enhanced activity because these mutations stabilize structural motifs of critical importance for receptor recognition.

The essential role of insulin in the hormonal control of metabolism has provided the impetus for extensive studies of structure–function relationships. Insulin is a 2-chain 51-residue globular protein and contains 1 intrachain and 2 interchain disulfide bridges (see Figure 1). The A-chain (21 residues) is composed of 2 helical segments (A2–A8 and A13–A19) joined by a loop in position A9–A11. X-ray studies of zinc–insulin hexamers (Baker et al., 1988; Derewenda et al., 1989) have shown that the B-chain of the insulin monomer can assume two distinct conformations. In the T-state conformation, residues B1–B8 take up an extended conformation, and residues B9–B19 form the central α-helix. In residues B20–B23, the B-chain makes a β-turn, and the C-terminal B24–B30 residues are in an extended β-conformation. In the R-state conformation, residues B1–B8 take up a helical conformation to form a region of helix contiguous from B1 to B19. The interconversion between various T- and R-states of the insulin hexamer has been shown to take place in solution (Renscheidt et al., 1984; Kaarsholm et al., 1989; Brader et al., 1991).

Recent studies of insulin structure–function relationships have emphasized the importance of the COOH-terminal β-strand of the B-chain, the central B-chain helix, and the NH_2-terminal A-chain helix in receptor binding interactions (Mirmira & Tager, 1989; Schwartz et al., 1987; Mirmira et al., 1991; Nakagawa & Tager, 1992). Significant overlap exists between these regions and those involved in insulin aggregation (Brange et al., 1988). In particular, upon dimerization the PheB24-PheB25-TyrB26 segment of one monomer forms an antiparallel β-sheet with the contiguous TyrB26-PheB25-PheB24 segment of the opposing monomer. In the presence of Zn^{2+} or other divalent metal ions, dimers aggregate further to form two-zinc insulin hexamers. This aggregate involves a distinct set of protein–protein contacts and the coordination of three HisB10 imidazolyl moieties to each zinc atom.

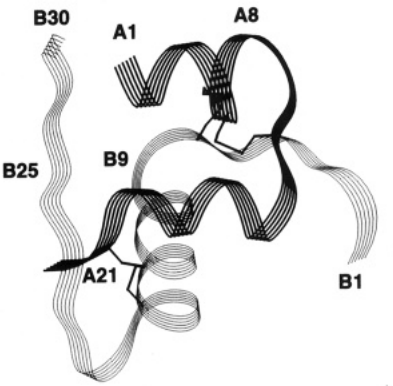

FIGURE 1: Diagrammatic structure of the T-state insulin monomer. The A-chain (solid black ribbon) contains one intrachain disulfide bridge (solid line) and is connected to the B-chain (stippled ribbon) via two interchain disulfide bridges (solid lines). Three regions of the molecule are analyzed in detail with respect to their contribution to folding stability, i.e., the C-cap of the initial A-chain helix (A8), the N-terminal region of the central B-helix (B9–B10), and the B25–B30 extended strand portion of the B-chain.

Clearly, the sequence and three-dimensional structure of insulin represent a successful compromise among requirements of a multitude of biochemical events that constitute insulin function. Prior to molecular recognition by the receptor, these events include protein folding and disulfide pairing, proteolytic processing of the prohormone, aggregation and stable storage as zinc–insulin hexamers, timely release of the biologically

* Address correspondence to this author at the Novo Research Institute, Novo Alle, Novo Nordisk A/S, DK-2880 Bagsvaerd, Denmark. Telephone: +45 4444 8888. Telefax: +45 4449 0555.

® Abstract published in *Advance ACS Abstracts,* September 15, 1993.

0006-2960/93/0432-10773$04.00/0

active monomeric species, and finally the efficient delivery to target cells.

In the present work, we focus on the folding stability of the insulin monomer. Site-directed mutagenesis is used to modify structure in selected regions of critical importance to various aspects of insulin function (cf. Figure 1). It is shown herein that the stability of the insulin fold may be enhanced by creation of hydrogen bonds, modifications near N- and C-caps of α-helices, and combinations thereof. Most importantly, it is found that mutations that provide strong stabilization of the A-chain NH_2-terminal helix and the central B-chain helix are identical with those that lead to enhanced biological activity of the insulin molecule.

MATERIALS AND METHODS

Materials. Native and mutant insulins were constructed by oligonucleotide-directed mutagenesis, fermented in yeast, and purified as described (Markussen et al., 1987; Brange et al., 1988). Guanidine hydrochloride (GuHCl)[1] (ultra pure grade) was obtained from Schwarz/Mann; Tris buffer was from Sigma. All other chemicals employed in these studies were reagent grade or better.

Methods. Protein concentrations were determined by UV absorbance using $\epsilon_{276} = 6.2 \times 10^3$ M^{-1} cm^{-1}. The same extinction coefficient was used for estimation of the concentration of mutant species with the assumption that each of the four tyrosines in human insulin contributes 25% to ϵ_{276}. Denaturation samples were prepared by combining different ratios of protein and GuHCl stock solutions with 10 mM Tris/ClO_4^- buffer, pH 8.0. Protein stock solutions were typically 1.5 mM in 10 mM Tris/ClO_4^-, pH 8.0. GuHCl stock solutions were 8.25 M (determined by refractometry) in 10 mM Tris/ClO_4^-, pH 8.0. The denaturations were found to reach equilibrium within 60 s after mixing and remained stable for at least 48 h. CD spectra were recorded with a Jobin-Yvon Mark V dichrograph calibrated with (+)-10-camphorsulfonic acid. All spectra were recorded at 25 °C. Far-UV CD denaturation samples were scanned from 250 to 218 nm. Typical cell path length and protein concentrations were 0.2 cm and 37 μM, respectively. Near-UV CD denaturation samples were scanned from 330 to 250 nm using 1-cm path length and typically 75 μM protein. All spectra were smoothed by a Fourier transform algorithm before subtraction of the appropriate solvent blanks. In the far-UV range, $\Delta\epsilon$ is based on the molar concentration of peptide bond, while in the near-UV $\Delta\epsilon$ is normalized to the molar concentration of insulin monomer.

Data Analysis. GuHCl denaturation curves were analyzed by assuming that the folding/unfolding transition is two-state, in which case equilibrium constants can be obtained at each denaturant concentration using $K = (\Delta\epsilon_N - \Delta\epsilon)/(\Delta\epsilon - \Delta\epsilon_U)$, where $\Delta\epsilon$ is the observed value of the CD and $\Delta\epsilon_N$ and $\Delta\epsilon_U$ represent the CD values for native and unfolded forms, respectively, at the given GuHCl concentration (Pace, 1975). Values for $\Delta\epsilon_N$ and $\Delta\epsilon_N$ at GuHCl concentrations in the transition region were obtained by linear extrapolation of the pre- and posttransition base lines into the transition region, i.e., $\Delta\epsilon_N = \Delta\epsilon^0_N + m_N$[GuHCl] and $\Delta\epsilon_U = \Delta\epsilon^0_U + m_U$[GuHCl], where $\Delta\epsilon^0_N$ and $\Delta\epsilon^0_U$ are intercepts and m_N and m_U are slopes of the pre- and posttransition base lines, respectively. The free energy of unfolding at a given denaturant concentration in the transition zone is given by

[1] Abbreviations: GuHCl, guanidine hydrochloride; CD, circular dichroism.

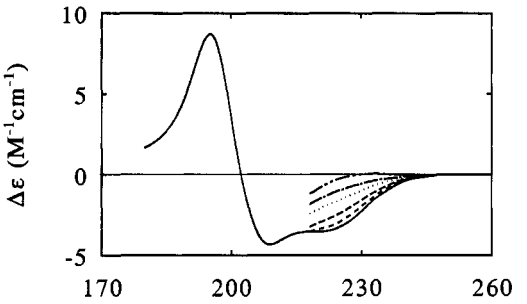

FIGURE 2: Far-UV CD spectrum of zinc-free human insulin at 100 μM in 10 mM Tris/ClO_4^-, pH 8.0, recorded from 180 to 260 nm using a 0.01-cm path length. Effect of increasing [GuHCl] on the 218–250-nm spectrum at 37 μM human insulin in 10 mM Tris/ClO_4^-, pH 8.0, recorded with a 0.2-cm path length, 25 °C. 0.82 (- - -), 3.26 (– –), 4.51 (···), 5.33 (– · –), and 7.74 (– ·· –) M GuHCl.

$\Delta G = -RT \ln K$. We assume a linear dependence of ΔG on denaturant concentration: $\Delta G = \Delta G_{H_2O} - m$[GuHCl], where ΔG_{H_2O} is the value of ΔG in the absence of denaturant and m is a measure of the dependence of ΔG on denaturant concentration. Hence, ΔG values derived from K in the transition zone may be extrapolated back to 0 M denaturant to give ΔG_{H_2O}. The relationship between $\Delta\epsilon$ and [GuHCl] for the complete unfolding curve is shown in eq 1 (Santoro & Bolen, 1988):

$$\Delta\epsilon = \{(\Delta\epsilon^0_N + m_N[\text{GuHCl}]) + (\Delta\epsilon^0_U + m_U[\text{GuHCl}]) \exp[-(\Delta G_{H_2O} - m[\text{GuHCl}])/RT)\}/\{1 + \exp[-(\Delta G_{H_2O} - m[\text{GuHCl}])/RT]\} \quad (1)$$

With $\Delta\epsilon$ as the response and [GuHCl] as the independent variable, eq 1 was subjected to nonlinear least-squares analysis using the NLIN procedure of PC SAS (SAS Inc., Cary, NC). Six parameters then describe the denaturation curve: $\Delta\epsilon^0_N$, $\Delta\epsilon^0_U$, m_N, m_U, m, and ΔG_{H_2O}. In addition, the GuHCl concentration at the midpoint of the denaturation curve, C_{mid}, is given by $\Delta G_{H_2O}/m$. The difference in the free energy of unfolding between human and mutant insulins may then be calculated from $\Delta\Delta G_{H_2O} = \Delta G_{H_2O(\text{mutant})} - \Delta G_{H_2O(\text{wild type})}$.

Free Fat Cell Assay (FFC). The potency of native and mutant insulins was estimated from their ability to enhance the incorporation of [2-^{3}H]glucose into lipids in isolated mouse adipocytes (Moody et al., 1974).

RESULTS

Analysis of the Far-UV CD Unfolding Curve for Native and Mutant Insulins. The CD observed below 240 nm is due to the peptide amide chromophore and may be used to estimate protein secondary structure (Johnson, 1985). The zinc-free human insulin spectrum (Figure 2) is characterized by minima at 220 and 209 nm, a negative to positive crossover near 203 nm, and a maximum at 195 nm. Upon denaturation, the negative CD in the 240–218-nm range gradually diminishes, consistent with the loss of ordered secondary structure that accompanies protein unfolding. The CD spectra of denaturated insulin are limited to these higher wavelengths by the denaturant absorption of light.

The far-UV CD spectrum of human insulin is sensitive to both protein unfolding and self-association (Holladay et al., 1977; Melberg & Johnson, 1990). In order to separate these phenomena at pH 8, GuHCl titrations were carried out at different protein concentrations. Figure 3 compares 224-nm unfolding curves at 3, 37, and 250 μM insulin, respectively. At these concentrations, insulin exists mainly as monomers

Table I: Folding Parameters and Biological Potencies for Native and Mutant Insulins

insulin	C_{mid}[a] (M)	m[a] (kcal mol^{-1} M^{-1})	ΔG_{H_2O}[a] (kcal/mol)	$\Delta\Delta G_{H_2O}$[b] (kcal/mol)	FFC potency[c] (human = 100%)
human					
monomers (3 μM)	4.37	0.86	3.76		
dimers (37 μM)	4.50 ± 0.05[d]	0.86 ± 0.02[d]	3.86 ± 0.05[d]		
oligomers (250 μM)	4.67	0.83	3.86		
mutant					
AspB9 near-UV (270 nm)	4.29	1.16	4.96		
AspB9 far-UV (224 nm)[e]	4.39	0.88	3.86	+0.10	26 (25–27)
AspB10	5.11	0.99	5.05	+1.30	207 (194–221)
GluB10	5.20	1.00	5.20	+1.44	402 (386–419)
ThrB10	4.66	0.76	3.54	–0.22	72 (70–74)
AlaA8	4.51	0.87	3.92	+0.16	112 (108–116)
HisA8	5.41	1.02	5.52	+1.76	309 (294–324)
ArgA8	4.77	1.05	5.01	+1.25	302 (286–342)
des-ThrB27	4.60	0.86	3.96	+0.20	168 (161–176)
des-TyrB26	4.38	0.78	3.42	–0.34	157 (150–164)
ThrB26	4.22	0.82	3.46	–0.30	58 (56–59)
des-(B26–B30)	4.23	0.80	3.38	–0.38	37 (35–39)
HisB25	4.91	0.97	4.76	+1.00	45 (43–46)
AspB25	4.74	0.92	4.36	+0.60	0.1 (0.09–0.11)
HisA8, AspB10, HisB25	6.05	1.14	6.90	+3.14	203 (196–210)

[a] Determined by a least-squares fit to eq 1 using sloping base lines (see Materials and Methods). [b] $\Delta G_{H_2O(mutant)} - \Delta G_{H_2O(human)}$. [c] Range indicates 95% confidence limits. [d] Mean ± SD of five determinations. The remaining numbers represent the mean of at least two determinations. [e] Stabilities for other mutants were determined by far-UV CD detection.

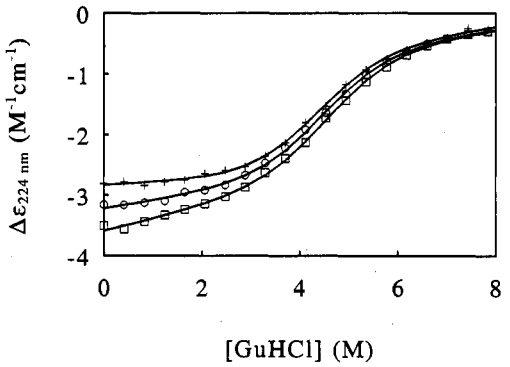

FIGURE 3: Far-UV CD unfolding curves of zinc-free human insulin as a function of protein concentration: 250 (□), 37 (○), and 3 μM (+) insulin. The solid lines represent the least-squares fit of the data to eq 1 using sloping base lines and the parameters listed in Table I.

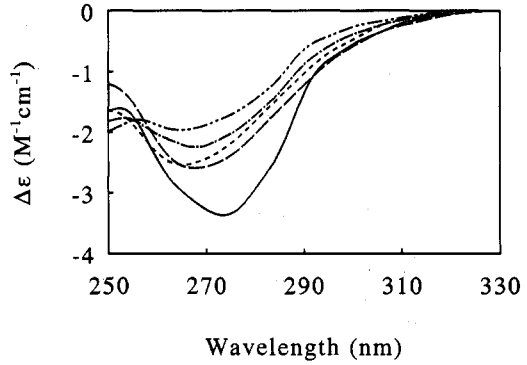

FIGURE 4: Near-UV CD spectra at 80 μM protein in 10 mM Tris/ClO_4^-, pH 8.0, recorded from 250 to 330 nm using a 1-cm path length. Human insulin (—), AspB9 monomeric insulin (- - -), and the effect of increasing [GuHCl] on the spectrum of AspB9: 2.0 (– –), 4.81 (– · –), and 7.43 (– ·· –) M GuHCl.

(3 μM), dimers (37 μM), and a mixture of dimers and higher aggregates (250 μM). A broad sigmoidal transition is observed at each protein concentration. The overlay with the insulin monomer ⇄ dimer equilibrium notably affects the slope and intercept of the pretransition base lines. For each protein concentration, the set of 250–218-nm CD spectra (Figure 2) were subtracted from that obtained in the absence of denaturant to produce a series of difference spectra as a function of [GuHCl]. Analysis of the difference spectra by singular value decomposition failed to resolve the transition in more than two stages (data not shown). Consequently, the dissociation into monomers occurs in the 0–3 M GuHCl region, but the accompanying change in the far-UV signal does not resolve into a separate transition and each unfolding curve is adequately fit by a two-state mechanism (eq 1).

Values of ΔG_{H_2O}, m, and C_{mid} for insulin at various concentrations are listed in Table I and show little effect of aggregation. Table I also shows the far-UV CD unfolding parameters for the B9-Ser → Asp analog where monomerization has been effected by mutation in the monomer–monomer interface without significant interference with the folding stability. Finally, the transitions illustrated in Figure 3 were found to be reversible; i.e., dilution of samples with high [GuHCl] to reduce denaturant concentration resulted in recovery of the expected CD (data not shown). We conclude that the unfolding transition of monomeric insulin is characterized by a low degree of cooperativity and a value of ΔG_{H_2O} which is on the low side for a globular protein (Pace et al., 1975).

Analysis of the Near-UV CD Unfolding Curve for Native and Mutant Insulins. In order to characterize the unfolding transition in more detail, near-UV CD was used to detect denaturation of human insulin and selected monomeric mutants. The insulin CD spectrum in the 330–250-nm range reflects the environment of the tyrosine chromophore with unknown contributions from the disulfide linkages (Morris et al., 1968; Goldman, 1971; Wood et al., 1975; Strickland & Mercola, 1976). The spectrum of the zinc-free species (Figure 4) is very sensitive to aggregation. The dimer exhibits a negative band with a minimum located at 273 nm. Monomerization leads to a loss of intensity and a shift in the minimum to about 265 nm. The effect of increasing [GuHCl] on the near-UV CD spectrum of monomeric B9-Ser → Asp insulin is shown in Figure 4. In the 0–2.5 M range, increasing [GuHCl] leads to a small increase in intensity and a 3-nm red-shift of the peak. At higher [GuHCl], the minimum gradually shifts back toward 266 nm, and the intensity of the peak progressively decreases, consistent with loss of tertiary structure. This result indicates that small conformational adjustments precede the unfolding reaction. Accordingly, in

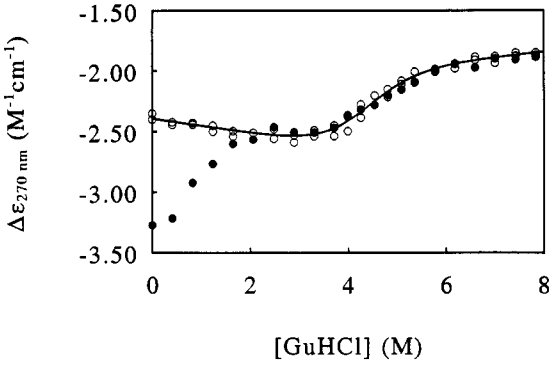

FIGURE 5: Near-UV CD unfolding curves for (●) 80 μM zinc-free human insulin (dimers) and (○) 80 μM monomeric AspB9 insulin in 10 mM Tris/ClO_4^-, pH 8.0. The solid line is calculated with eq 1 using sloping base lines and the parameters listed in Table I.

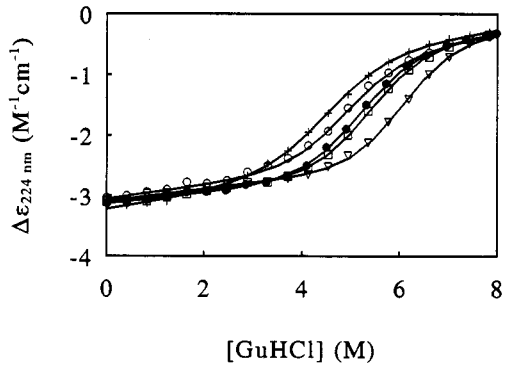

FIGURE 6: Far-UV CD unfolding curves for native and mutant insulins at 37 μM protein, and 25 °C. (+) Human insulin; (○) HisB25; (●) AspB10; (□) HisA8; (▽) HisA8, AspB10, and HisB25 insulins. The solid lines are calculated with eq 1 using sloping base lines and the parameters listed in Table I.

the plot of $\Delta\epsilon$ vs [GuHCl], the slope of the pretransition base line is dependent on the wavelength chosen (data not shown). Nevertheless, at each wavelength, the unfolding curve fits a two-state transition (eq 1), and the values of ΔG_{H_2O}, m, and C_{mid} (Table I) are not significantly dependent on the wavelength in the 260–275-nm range. Figure 5 compare near-UV CD unfolding curves for human insulin and the B9-Ser → Asp monomer. In the 0–3 M GuHCl range, human insulin dissociates into monomers, while at higher concentrations of denaturant unfolding of the monomer is observed. Note that the second phase for human insulin is indistinguishable from the unfolding transition of the B9-Ser → Asp monomeric insulin.

For the AspB9 species (Table I), the values of both ΔG_{H_2O} and m are about 22–24% larger than those obtained by using far-UV CD detection. However, because both parameters increase by about the same factor, the value of C_{mid} is nearly independent of the method of detection.

Analysis of Unfolding Curves for Mutant Insulins. As documented above, the near- and far-UV CD unfolding curves for human and monomeric AspB9 insulins are both adequately analyzed employing the two-state approximation. However, the significantly different values of ΔG_{H_2O} and m obtained with the two detection methods indicate that the transition deviates from the two-state model and that folding intermediates may be present. For comparison of the folding stability between insulin mutants presented below, we have employed far-UV CD detection because the signal is larger and because small differences in the aggregation state cause only minor changes in ΔG_{H_2O} and m (cf. Figure 3 and Table I). Examples of far-UV CD unfolding curves for mutant insulins are shown in Figure 6.

Central α-Helix of the B-Chain. The α-helix of the T-state B-chain (B9–B19) is important to several structural characteristics of the insulin molecule. The helix contains invariant LeuB11 and LeuB15 residues which are part of the hydrophobic core of the monomer. Residue HisB10 contributes ligand to Zn^{2+} in the formation of zinc–insulin hexamers, and the N-terminal part of the helix is near the hinge region for the T to R transition (Figure 1). The contribution of the N-terminal residues to the stability of the B9–B19 helix was examined by introducing negative charge in position SerB9 and by exchange of HisB10 with neutral and negatively charged residues. As shown in Figure 4 and Table I, introduction of negative charge in the side chain of B9 has essential no effect on the folding stability. In contrast, substitution of HisB10 with either Glu or Asp leads to substantial enhancement of both ΔG_{H_2O} and m, while mutation of HisB10 to Thr lead to a small decrease in both parameters. Note that the mutations conferring enhancement of helix stability (AspB10, GluB10) are identical to those that enhance the *in vitro* biological potency (Table I).

NH_2-Terminal α-Helix of the A-Chain. The first residues of the A-chain are known to be important for receptor interactions [see, e.g., Nakagawa and Tager (1992) and references cited therein]. In this region, the X-ray structure shows differences between monomer molecules 1 and 2 of the insulin dimer (Baker et al., 1988). The difference is due to a 32° rotation about the CysA6 C^{α}–NH bond in molecule 2 relative to molecule 1, which carries with it the initial five residues of the A-chain. This rotation introduces different hydrogen-bonding patterns in the helix. We examined the stability of the A2–A8 helix by mutating the C-cap ThrA8 to Ala, Arg, and His, respectively. While the ThrA8 → Ala mutation has little or no effect on folding stability, mutation to His and Arg in this position both lead to a remarkable enhancement of m and ΔG_{H_2O}. Again, the enhanced stability is associated with enhanced biological activity (cf. Table I).

COOH-Terminal Part of the B-Chain. The C-terminal segment (B24–B30) of the insulin molecule exists in an extended conformation (Figure 1). The hydrophobic cluster, PheB24-PheB25-TyrB26, is exposed in the monomer and part of the surface that becomes buried upon dimerization. Various X-ray structures show that the C-terminal residues B29–B30 are disordered, indicating some degree of flexibility in this region. As shown in Table I, deletion of ThrB27 results in an insulin molecule with slightly enhanced folding stability. Substitution of TyrB26 with Thr and deletion of TyrB26 both lead to significant decreases in m and ΔG_{H_2O}. The destabilizing effect of these modifications is similar to that produced by deletion of the entire B25–B30 pentapeptide segment. Finally, as shown in Table I, a considerable increase in the folding stability of the full-length monomer may be accomplished by mutation of PheB25 to either Asp or His. Note that for modifications in the B25–B30 region, our data show no correlation between global folding stability and bioactivity. Enhanced potency may be associated with increased (des-ThrB27) or reduced (des-TyrB26) folding stability, and species with decreased potency may be either more (AspB25) or less (ThrB26) stable than the wild type (Table I).

Additivity of Stabilizing Mutations. The independence of stabilizing mutations in the three regions examined was tested by combining mutations ThrA8 → His, HisB10 → Asp, and PheB25 → His into a single insulin species. As shown in Table I, this combination results in a mutant where the

equilibrium constant between folded and unfolded forms is shifted about 200-fold in favor of the folded state in comparison with the wild type. This result indicates that stabilizing mutations in these three regions are essentially independent. Similarly, the three mutations affect the biological potency in a nearly independent fashion. This result further underscores the biological importance of folding stability in the NH_2-terminal A-chain and the central B-chain helices, while in the COOH-terminal of the B-chain the correlation between these phenomena is less clear.

Finally, for the full-length insulin species listed in Table I, regression analysis showed a strong linear correlation (r^2 = 0.95) between the two-state folding parameters m and ΔG_{H_2O}. This linear correlation shows that enhanced stability generally is accompanied by enhanced cooperativity of the unfolding transition.

DISCUSSION

Folding Intermediates. The unfolding parameters for the insulin monomer exhibit small but significant differences depending on the method of detection. This result and the observation of subtle changes in the near-UV CD spectrum at low [GuHCl] (Figure 4) lead to the conclusion that intermediates are present on the unfolding pathway. The direct correlation between m and ΔG_{H_2O} for the full-length mutants provides further evidence that the unfolding transition is not exactly two-state. Thus, it is likely that increased values of m reflect relative destabilization of intermediates that otherwise exist in the low [GuHCl] range. The folding stability of human insulin has previously been studied by near- and far-UV CD using a mixed ethanol/H_2O [20/80 (v/v)] solvent system (Brems et al., 1990). However, due to the perturbing effect of the cosolvent, it is not possible to quantitatively compare these data with those described here. Nevertheless, the value of ΔG = 4.5 ± 0.5 kcal/mol reported by Brems et al. (1990) is in general agreement with the results presented here. Similarly, by using the same solvent, Bryant et al. (1992) recently reported the detection of an equilibrium intermediate in the GuHCl-induced unfolding of the TrpB28, ProB29 insulin mutant.

Capping and α-Helix Stability. The first and the last four residues of α-helices generally differ from the rest in not being able to make the intrahelical hydrogen bonds between the backbone >C=O groups of one turn and the >NH groups of the next (Presta & Rose, 1988; Richardson & Richardson, 1988; Serrano & Fersht, 1989). The insulin X-ray structure shows that due to bifurcated hydrogen-bonding patterns, the backbone NH's of GlyB8 and SerB9 are the only unpaired main-chain hydrogen bond donors in the first turn of the central B-chain helix (Baker et al., 1988). Modeling studies show that aspartate side chains in positions B9 or B10 are unable to form favorable hydrogen bonds with the unpaired backbone NH's of either GlyB8 or SerB9. In contrast, the side chains of Asp or Glu in position B10 (but not position B9) can rotate to bring the negative charge ito favorable interaction with the helix dipole. Close to this position is an additional favorable interaction involving a hydrogen bond between the B10 side-chain carbonyl oxygen and the backbone >NH of CysB7 outside the helix. These stabilizing structural motifs are illustrated in Figure 7a,b. In principle, the Oγ of ThrB10 is capable of forming a similar hydrogen bond to the NH of CysB7; however, this arrangement would result in the unfavorable exposure of the side chain methyl group to the solvent. Accordingly, the folding stability of the ThrB10 species is less than or comparable to that of the wild type.

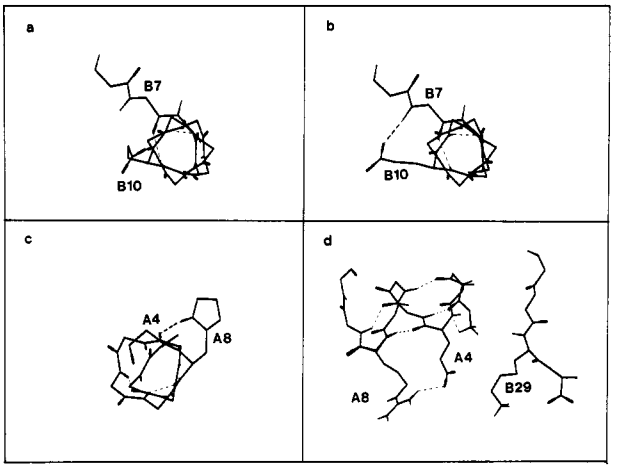

FIGURE 7: Stabilizing interactions at the N-cap of the central B-chain helix and the C-cap of the NH_2-terminal A-chain helix. Parts a and b illustrate views down the B9–B19 α-helix with the side chain of GluB10 either interacting with the helix dipole (a) or forming a hydrogen bond with the backbone >NH of CysB7 (b). Part c shows the initial α-helix of the A-chain and the formation of a hydrogen bond between the C-cap imidazolyl side chain of HisA8 and the main chain >C=O of GluA4. Part d shows the additional stabilizing interaction in the ArgA8 species where the carboxylate of GluA4 becomes sandwiched between positive charges of LysB29 and ArgA8 side chains. This latter interaction is modeled on the basis of molecule 2 of the X-ray structure.

In the N-terminal A-chain helix, modeling studies indicate that the most plausible explanation for the enhanced stability of the HisA8 species is the formation of a hydrogen bond between the A8 imidazolyl side chain and the backbone carbonyl of GluA4. This structural motif is illustrated in Figure 7c. Note that the side chain of the native ThrA8 can only donate this hydrogen bond by simultaneous exposure to the solvent of the methyl group. Accordingly, AlaA8 is as stable as the wild type. Arginine in position A8 is also capable of donating hydrogen bond to >C=O of GluA4; however, in this case, two additional stabilizing interactions are possible. One involves the interaction of the positively charged arginine side chain with the α-helix dipole; the other can be modeled on the basis of molecule 2. In this structure, the side chains of LysB29 and GluA4 interact to maintain the C-terminus of the B-chain in close proximity to the NH_2 terminus of the A-chain. The guanidium moiety of the ArgA8 mutant is in perfect position to sandwich the Glu4 carboxylate between the positively charged side chains of LysB29 and ArgA8 as illustrated in Figure 7d. Note that this latter interaction would tighten the COOH-terminal of the B-chain to the body of the molecule. Nevertheless, the relatively potency of this species is 302% (Table I).

COOH-Terminus of the B-Chain. The X-ray structure shows that the PheB25 side chain exists in two distinct conformations. In molecule 1, it turns toward the A-chain touching TyrA19, while in molecule 2 it turns out from the molecule exposing the side chain to the solvent. The side chain of TyrB26 is directed internally where it packs against ProB28 on one side and PheB24 on the other (Baker et al., 1988). This arrangement suggests that the stabilizing effect of B25Asp and His mutations is due to a reduction of hydrophobic surface area in the folded monomer. For the HisB25 species, an additional stabilizing interaction may be obtained by the formation of a hydrogen bond between the

side chain and the backbone carbonyl of TyrA19. For the B26 residue, the gain in stability resulting from reduction ofthe hydrophobic surface area in the folded state is expected to be smaller, and the loss of stabilizing interactions from the tyrosine side chain actually leads to a slight net destabilization in the ThrB26 species. By analogy, deletion of the B26 residue is expected to decrease folding stability due to loss of B24–B26 aromatic–aromatic interactions. These interactions are restored in the des–B27 mutant which actually exhibits somewhat greater folding stability than the wild type. This phemomenon is most reasonably explained by assuming that TyrB26 orients the shorter terminus of the B-chain to provide enhanced potential for ionic interactions involving the side chains of LysB29 with GluA4 and/or the carboxylate of ThrB30 with the NH_2-terminal GlyA1.

Folding Stability and Biological Activity. The enhanced biological potency of HisA8 and AspB10 mutants has been reported previously (Marki et al., 1979; Schwartz et al., 1987). We conclude that these and similar modifications (ArgA8 and GluB10) elicit enhanced activity because they stabilize structural motifs of critical importance for receptor recognition, i.e., the NH_2-terminal A-chain and the central B-chain helices. In the AspB9 species, the decreased activity despite retention of native folding stability illustrates that mutations near sites of direct receptor contact add to the importance of helix stability.

The relationship between bioactivity and structural stability in the COOH-terminal part of the B-chain is less clear. For example, on the basis of NMR of measurements in the presence of 20% acetic acid at pH 2.2, Hua et al. (1991, 1993) have reported that the B20–B30 segment is unfolded in the biologically active GlyB24 mutant while near-native fold is retained for the essentially inactive SerB24 species. Insulin receptor binding is thought to involve small adjustments of the main chain structure in the B25–B30 region of the molecule (Mirmira et al., 1991). It is likely that such minor changes in the main chain conformation would have relatively little effect on the global folding stability measured here; cf. the small destabilization observed for the des-B26–B30 species.

In conclusion, we have focused on structural stability in three regions of the insulin molecule which are thought to be important in receptor binding interactions. Although the total number of sites examined is obviously too small to imply correlations between biological activity and stability of the insulin fold in general, our data clearly emphasize the functional importance of structural stability in selected helical segments of the insulin molecule. In the receptor binding reaction, the intrinsic binding energy is used to force the receptor to change to the active form that is capable of initiating transmembrane signaling. Because the interaction energies level the Gibbs energy profile for the receptor–ligand reaction in order to avoid large energy wells and barriers along the reaction path, it is likely that structural flexibility in the insulin molecule functions to destabilize the insulin–receptor complex after internalization. In other words, insulin mutants such as GluB10 or HisA8 would have an increased energy barrier for receptor dissociation and hence suboptimal function *in vivo*.

ACKNOWLEDGMENT

We thank Susan E. Danielsen and Anne-Marie Kolstrup for expert technical assistance throughout this work.

REFERENCES

Baker, E. N., Blundell, T. L., Cutfield, J. F., Cutfield, S. M., Dodson, E. J., Dodson, G. G., Hodkin, D. M. C.; Hubbard, R. E., Isaacs, N. W., Reynolds, C. D., Sakabe, K., Sakabe, N., & Vijayan, N. M. (1988) *Philos. Trans. R. Soc. London 319*, 369–456.

Brader, M. L., Kaarsholm, N. C., Lee, R. W.-K., & Dunn, M. F. (1991) *Biochemistry 30*, 6636–6645.

Brange, J., Ribel, U., Hansen, J. F.; Dodson, G., Hansen, M. T., Havelund, S., Melberg, S. G., Norris, K., Norris, F., Snel, L., Sørensen, A. R., & Voigt, H. O. (1988) *Nature 333*, 679–682.

Brems, D. N., Brown, P. L., Heckenlaible, L. A., & Frank, B. H. (1990) *Biochemistry 29*, 9289–9293.

Bryant, C., Strohl, M., Green, K., Long, H. B., Alter, L. A., Pekar, A. H., Chance, R. E., & Brems, D. N. (1992) *Biochemistry 31*, 5692–5698.

Derewenda, U., Derewenda, Z., Dodson, E. J., Dodson, G. G., Reynolds, C. D., Smith, G. D., Sparks, C., & Swensen, D. (1989) *Nature 338*, 594–596.

Goldman, J. (1971) Ph.D. Dissertation, University of California, Berkerly.

Holladay, L. A., Ascoli, M., & Puett, D (1977) *Biochim. Biophys. Acta 494*, 245–254.

Hua, Q. X., Shoelson, S. E., Kochoyan, M., & Weiss, M. A. (1991) *Nature 354*, 238–241.

Hua, Q. X., Shoelson, S. E., Inouye, K., & Weiss, M. A. (1993) *Proc. Natl. Acad. Sci. U.S.A. 90*, 582–586.

Johnson, W. C., Jr. (1988) *Annu. Rev. Biophys. Chem. 17*, 145–166.

Kaarsholm, N. C., Ko, H.-C., & Dunn, M. F. (1989) *Biochemistry 28*, 4427–4435.

Marki, F., De Gasparo, M., Eisler, K., Kamber, B., Riniker, B., Rittel, W., & Sieber, P. (1979) *Hoppe-Seyler's Z. Physiol. Chem. 360*, 1619–1632.

Markussen, J., Diers, I., Engesgaard, A., Hansen, M. T., Hougaard, P., Langkjaer, L., Norris, K., Ribel, U., Sørensen, A., Sørensen, E., & Voigt, H. O. (1987) *Protein Eng. 1*, 215–223.

Melberg, S. G., & Johnson, W. C., Jr. (1990) *Proteins: Struct., Funct., Genet. 8*, 280–286.

Mirmira, R. G., Nakagawa, S. H., & Tager, H. S. (1991) *J. Biol. Chem. 266*, 1428–1436.

Moody, A. J., Stan, M. A., & Stan, M. (1974) *Horm. Metab. Res. 6*, 12–16.

Morris, J. W. S., Mercola, D., & Arquilla, E. R. (1968) *Biochim. Biophys. Acta. 160*, 145–155.

Nakagawa, S. H., & Tager, H. S. (1991) *J. Biol. Chem. 266*, 11502–11509.

Nakagawa, S. H., & Tager, H. S. (1992) *Biochemistry 31*, 3204–3214.

Pace, C. N. (1975) *CRC Crit. Rev. Biochem. 3*, 1–43.

Presta, L. G., & Rose, G. D. (1988) *Science 240*, 1632–1641.

Renscheidt, H., Strassburger, W., Glatter, U., Wollmer A., Dodson, G., & Mercola, D. A. (1984) *Eur. J. Biochem. 142*, 7–14.

Richardson, J. S., & Richardson, D. C. (1988) *Science 240*, 1648–1652.

Santoro, M. M., & Bolen, D. W. (1988) *Biochemistry 27*, 8063–8068.

SAS Institute Inc. (1987) SAS/STAT Guide for Personal Computers, Version 6, pp 675–712, SAS Institute, Cary, NC.

Schwartz, G. P., Burke, G. T., & Katsoyannis, P. G. (1987) *Proc. Natl. Acad. Sci. U.S.A. 84*, 6408–6411.

Serrano, L., & Fersht, A. R. (1989) *Nature 342*, 296–299.

Strickland, E. H., & Mercola, D. (1976) *Biochemistry 15*, 3875–3884.

Wood, S. P., Blundell, T. L., Wollmer, A., Lazarus, N. R., & Neville, R. W. J. (1975) *Eur. J. Biochem. 55*, 531–542.